

Discontinuous Galerkin method based on the reduced space for the nonlinear convection-diffusion-reaction equation

Shijin Hou* Yinhua Xia†

Abstract

In this paper, by introducing a reconstruction operator based on the Legendre moments, we construct a reduced discontinuous Galerkin (RDG) space that could achieve the same approximation accuracy but using fewer degrees of freedom (DoFs) than the standard discontinuous Galerkin (DG) space. The design of the “narrow-stencil-based” reconstruction operator can preserve the local data structure property of the high-order DG methods. With the RDG space, we apply the local discontinuous Galerkin (LDG) method with the implicit-explicit time marching for the nonlinear unsteady convection-diffusion-reaction equation, where the reduction of the number of DoFs allows us to achieve higher efficiency. In terms of theoretical analysis, we give the well-posedness and approximation properties for the reconstruction operator and the L^2 error estimate for the semi-discrete LDG scheme. Several representative numerical tests demonstrate the accuracy and the performance of the proposed method in capturing the layers.

Keywords: reduced discontinuous Galerkin space, Legendre moments, local discontinuous Galerkin method, unsteady convection-diffusion-reaction equation.

1 Introduction

In this paper, we consider the following nonlinear unsteady convection-diffusion-reaction (CDR) equation

$$u_t + \nabla \cdot (\mathbf{b}(\mathbf{x})f(u)) - \varepsilon \Delta u + r(u) = g(\mathbf{x}, t), \quad (\mathbf{x}, t) \in \Omega \times (0, T], \quad (1.1a)$$

$$u(\mathbf{x}, 0) = u_0(\mathbf{x}), \quad \mathbf{x} \in \overline{\Omega}, \quad (1.1b)$$

where the diffusion velocity ε is positive, the convection velocity field $\mathbf{b}(\mathbf{x})$, $f(u)$, $r(u)$ and $g(\mathbf{x}, t)$ are smooth, the initial solution u_0 belongs to $L^2(\Omega)$, and Ω is a bounded domain

*School of Mathematical Sciences, University of Science and Technology of China, Hefei, Anhui 230026, People’s Republic of China. Email: houshiji@mail.ustc.edu.cn.

†School of Mathematical Sciences, University of Science and Technology of China, Hefei, Anhui 230026, People’s Republic of China. Email: yhxia@ustc.edu.cn. This author was partially supported by National Natural Science Foundation of China grant No. 12271498

in \mathbb{R}^d with the dimension d . With various appropriate boundary conditions, it yields a well-posed problem. The CDR equation has always received considerable attention as a model for fluid flow and heat transfer problems. It is widely applied in various fields of science and engineering such as chemical process simulation, river pollution, reservoir simulation, financial problems, etc [23, 24]. Among these applications, a challenging scenario arises when numerically solving a convection-dominated or reaction-dominated type of CDR equation (i.e., $\varepsilon \ll 1$) whose solution may suffer from sharp internal or boundary layers [18]. In such cases, the standard finite element method leads to spurious numerical oscillations. In order to overcome this, a number of stabilized numerical methods have been developed, such as the streamline upwind Petrov-Galerkin (SUPG) [5, 3], the Gaussian radial basis function (RBF) [19, 22], etc.

In recent decades, the discontinuous Galerkin (DG) methods have been proposed as a kind of robust, accurate method for numerically solving the convection-dominated problem and have received a lot of research [9]. It can capture the interior or boundary layers well thanks to two aspects: First, by adopting the discontinuous basis space, DG methods can more flexibly describe the complicated structure of the solution near the layers. Second, the numerical flux naturally guarantees the upwind property. In addition, DG methods have many advantages, such as high parallel efficiency, easy implementation on complicated geometries, etc. Thus, a range of DG methods has been proposed for the CDR equation. Paul et al. developed the *hp*-version DG method for several second-order partial differential equations with nonnegative characteristic forms [16]. Ayuso et al. applied the weighted-residual approach to derive the DG scheme for the steady state CDR equation in [2]. Nguyen et al. presented the implicit high-order hybridizable DG methods for the time-dependent nonlinear convection-diffusion (CD) equations [21]. Cockburn and Shu studied the Runge-Kutta discontinuous Galerkin (RKDG) method for the time-dependent convection-dominated parabolic problems [12]. As an extension of the RKDG method, they proposed the Local Discontinuous Galerkin (LDG) methods for nonlinear time-dependent CD systems [11]. Xu et al. provided L^2 error estimates for the semi-discrete LDG method for nonlinear CD equations [29]. Wang et al. analyzed the stability and error estimation of the implicit-explicit (IMEX) LDG method for multi-dimensional nonlinear CD equation [27]. However, all the above DG methods suffer from considerable degrees of freedom (DoFs), which could lead to higher computational costs than the traditional finite element methods (FEMs).

Therefore, several improved methods have been developed to reduce the number of DoFs. Cockburn et al. developed a hybridizable DG method for the steady-state CDR equation [8]. Recently, Li et al. proposed a novel approach based on the patch reconstruction discontinuous Galerkin space, in which the arbitrary high-order DG methods have only one degree of freedom per element [20]. This method has been used to solve the steady-state CD equation in [25]. Its excellent performance in reducing the number of DoFs is widely recognized. However, high-order reconstruction requires a wide stencil according to the strategy in [20]. In this case, the local data structure property of the DG methods is weakened to some extent.

In this article, we aim to propose an efficient DG method for the nonlinear unsteady CDR equation. Our first contribution is to propose a reconstruction operator using the Legendre moments [30]. Here, we consider a fixed narrow stencil consisting only of the

element itself and its direct neighbors, instead of the wide stencil used in [20], and implement the high-order reconstruction by exploiting the high-order Legendre moments on each element of the stencil. In addition, we study the well-posedness and some approximation properties of this reconstruction operator for our later analysis. Applying this operator, we construct the reduced discontinuous Galerkin (RDG) space which is able to use reduced DoFs to achieve the same approximation accuracy as the standard DG space. It's worth noting that the high-order reconstruction approach based on a narrow stencil can well preserve the local data structure property of DG methods. In light of the above advantages, we can develop some efficient DG methods based on this RDG space. In the second part, we apply the LDG method based on our RDG space for spatial discretization and provide the error estimation for the semi-discrete LDG scheme. Combined with the implicit-explicit Range-Kutta (IMEX RK) time discretization method, we propose the complete IMEX RK LDG method. In the IMEX RK scheme, the diffusion part is treated implicitly, which avoids the severe step restriction but introduces a large linear system to be solved at each time step, showing that our RDG space can effectively reduce the computational cost.

The paper is organized as follows. In Section 2, we introduce the notations, definitions, and preliminaries used later in the paper. In Section 3, we define the compact reconstruction operator and present some approximation properties of it. Using this operator, we also give the definition of the RDG space. In Section 4, the IMEX RK LDG method is applied to solve the nonlinear CDR equation. In addition, the error estimate is derived in the L^2 norm. In Section 5, we present numerical results for several one-and two-dimensional CDR equations to demonstrate the accuracy. Finally, we draw the conclusion in Section 6.

2 Notation and preliminaries

For an open and bounded domain $K \subset \mathbb{R}^d$, let $W^{s,p}(K)$ with indexes $s \geq 0$, $1 \leq p \leq \infty$ denote the Sobolev space of functions whose derivatives up to order s belong to the space $L^p(K)$. Its seminorm and norm are denoted by $|\cdot|_{s,p,K}$ and $\|\cdot\|_{s,p,K}$ respectively. In the most common case, $p = 2$, we write $H^s(K)$ instead of $W^{s,2}(K)$ for simplicity and denote the corresponding seminorm and norm by $|\cdot|_{s,K}$ and $\|\cdot\|_{s,K}$. For $s = 0$, $H^s(K)$ coincides with $L^2(K)$. Hence the norm and inner product of $L^2(K)$ can be denoted by $\|\cdot\|_{0,K}$ and $(\cdot, \cdot)_K$. Moreover, Let $P^k(K)$ denote the space of polynomials of degree at most k on K .

Consider a d -dimensional hypercube $\Omega = \prod_{i=1}^d [a_i, b_i]$ and let \mathcal{T}_h denote the rectangular partition with disjoint N elements. Assuming that we distribute N_i elements on the i th direction, i.e., $[a_i, b_i] = \cup_{j=1}^{N_i} I_j^i$, where $I_j^i = [x_{j-\frac{1}{2}}^i, x_{j+\frac{1}{2}}^i]$. Thus we have $N = \prod_{i=1}^d N_i$. Here we define a set of multiple indicators, $\Theta^d = \{\theta = (\theta_1, \dots, \theta_d) | 1 \leq \theta_i \leq N_i, i = 1, \dots, d\}$. For each $\theta \in \Theta^d$, the θ th element is denoted by $K_\theta = \prod_{i=1}^d I_{\theta_i}^i$. The corresponding center point is denoted by $\mathbf{x}_\theta = (x_\theta^1, \dots, x_\theta^d)$ with $x_\theta^i = (x_{\theta_i-\frac{1}{2}}^i + x_{\theta_i+\frac{1}{2}}^i)/2$. Let \mathcal{E}_h denote the set of all edges of elements in \mathcal{T}_h , and $\mathcal{E}_h^0 = \mathcal{E}_h \setminus \partial\Omega$ denote the set of interior edges. Moreover, for every $K \in \mathcal{T}_h$, we denote its area by $|K|$ and the element length in

i th direction by h_K^i . Naturally, we can define the maximum and minimum mesh size by

$$h = \max_{K \in \mathcal{T}_h, 1 \leq i \leq d} h_K^i, \quad \underline{h} = \min_{K \in \mathcal{T}_h, 1 \leq i \leq d} h_K^i.$$

We assume that \mathcal{T}_h is regular: With mesh refinements, there always exists a real positive number γ independent of h such that the ratio of the maximum and the minimum mesh size can be bounded by γ , i.e., $h \leq \gamma \underline{h}$.

Given the mesh \mathcal{T}_h , we denote by $Q^k(K)$ the tensor product piecewise polynomials of degree at most k in each variable on the element K . Then, a piecewise polynomial space can be defined as:

$$V_h^k = \{v \in L^2(\Omega) : v|_K \in Q^k(K), \forall K \in \mathcal{T}_h\},$$

which is the general discontinuous Galerkin space.

Based on the regularity assumption, there are several useful properties that will be used for the later analysis. For convenience to description, we denote by C a positive constant which may depend on the regularity of the function and the regularity parameter γ but is independent of h and adopt it to represent all scaling constants with the same characters in this paper.

Agmon's inequality For any $v \in H^1(K)$, there exists a positive constant C such that

$$\|v\|_{0,\partial K}^2 \leq C (h^{-1}\|v\|_{0,K}^2 + h|v|_{1,K}). \quad (2.2)$$

Approximation property For any $v \in H^{k+1}(K)$, there exists an approximation $v_h \in P^k(K)$ satisfying

$$\|v - v_h\|_{0,K} + h|v - v_h|_{1,K} \leq Ch^{k+1}|v|_{k+1,K}. \quad (2.3)$$

Inverse properties For any $v_h \in V_h^k$, there exists a positive constant C such that

$$\|\partial_x v_h\|_{0,K} \leq Ch^{-1}\|v_h\|_{0,K}, \quad (2.4a)$$

$$\|v_h\|_{0,\partial K} \leq Ch^{-\frac{1}{2}}\|v_h\|_{0,K}, \quad (2.4b)$$

$$\|v_h\|_{0,\infty,K} \leq Ch^{-\frac{d}{2}}\|v_h\|_{0,K}. \quad (2.4c)$$

Agmon's inequality (2.2) has been proved in [13]. More details of inverse properties (2.4) can be seen in [7].

3 Reduced discontinuous Galerkin space

In this section, we introduce the compact reconstruction operator by employing the Legendre moments on a fixed narrow stencil for the cases $d = 1, 2$. Moreover, we give the well-posedness condition and some approximation properties for the reconstruction operator, which is critical to the error estimate later. In the end, we define the reduced discontinuous Galerkin (RDG) space by applying this reconstruction operator.

3.1 Reconstruction operator

Let us start by introducing a fixed narrow element stencil. In the case of one dimension, we select the element itself and its two neighbor elements as the stencil. Given the mesh $\mathcal{T}_h = \{K_j\}_{j=1}^N$, the element stencil for periodic boundary value problems can be denoted as follows:

$$S^1(K_j) = \{K_{j-1}, K_j, K_{j+1}\}, \quad j = 1, \dots, N,$$

where K_0, K_{N+1} are obtained by the periodic extension. For other non-periodic boundary conditions, we denote the following bias stencil

$$\begin{aligned} S^1(K_1) &= \{K_1, K_2, K_3\}, \\ S^1(K_j) &= \{K_{j-1}, K_j, K_{j+1}\}, \quad j = 2, \dots, N-1, \\ S^1(K_N) &= \{K_{N-2}, K_{N-1}, K_N\}. \end{aligned}$$

For two dimensions, the stencil is given by the tensor product of the one-dimensional stencil defined above. Consider the mesh $\mathcal{T}_h = \{K_\theta \mid \theta \in \Theta^2\}$, where $K_\theta = I_{\theta_1}^1 \times I_{\theta_2}^2$ as denoted in the previous section. Here, we can define the one-dimensional stencil for the first direction by $\{S^1(I_{\theta_1}^1)\}_{\theta_1=1}^{N_1}$, similarly, $\{S^1(I_{\theta_2}^2)\}_{\theta_2=1}^{N_2}$ for the second direction. The two-dimensional stencil is defined by

$$S^2(K_\theta) = S^1(I_{\theta_1}^1) \times S^1(I_{\theta_2}^2).$$

In what follows, for any $K \in \mathcal{T}_h$, we denote the stencil by $S(K)$ without distinguishing one or two dimensions.

Given the standard Legendre basis functions $\{\widehat{L}^i(\widehat{x})\}_{i=0}^k$ for $\widehat{x} \in [-1, 1]$, we denote the multiple dimensional Legendre basis functions of degree $(\sum_{i=1}^d \alpha_i)$ on element K by

$$L_K^\alpha(\mathbf{x}) = \prod_{i=1}^d \widehat{L}^{\alpha_i} \left(\frac{2(x_i - x_{\theta_i})}{h_K^i} \right).$$

Here $\alpha = (\alpha_1, \dots, \alpha_d)$ is a multiple indicator belonging to $A^k = \{(\alpha_1, \dots, \alpha_d) \mid 0 \leq \alpha_i \leq k\}$. For $\alpha \in A^k$ and the element K , the Legendre moments of order $(\sum_{i=1}^d \alpha_i)$ for a function $u \in C^0(K)$ are defined as [30]:

$$I_K^\alpha u(\mathbf{x}) = \left(\prod_{i=1}^d \frac{2\alpha_i + 1}{h_K^i} \right) \int_K L_K^\alpha(\mathbf{x}) u(\mathbf{x}) d\mathbf{x}.$$

These Legendre moments can provide sufficient information to determine an interpolating approximation for u . By simple computation, we can verify that the following polynomial $p(\mathbf{x}) \in Q^k(K)$ with the Legendre series expansion form

$$p(\mathbf{x}) = \sum_{\alpha \in A^k} I_K^\alpha u(\mathbf{x}) \prod_{i=1}^d \widehat{L}^{\alpha_i} \left(\frac{2(x_i - x_{\theta_i})}{h_K^i} \right)$$

¹The k th order Legendre polynomials are defined as: $\widehat{L}^k(\widehat{x}) = \frac{(-1)^k}{2^k k!} \left(\frac{d}{dx} \right)^k [(1-x^2)^k]$ [1].

is a $(k + 1)$ th order approximation for u in the L^2 norm. The coefficients of $p(\mathbf{x})$ are determined by solving an approximation problem as follows

$$I_K^\alpha p(\mathbf{x}) = I_K^\alpha u(\mathbf{x}), \quad \forall \alpha \in A^k.$$

We aim to define a local reconstruction operator R_K^k which generates a $(k + 1)$ th order approximation polynomial $R_K^k u \in P^k(S(K))$ for a piecewise continuous function u . Inspired by the above interpolation problem, we consider using several low-order Legendre moments on each element of the stencil $S(K)$ to determine the high-order approximation polynomial $R_K^k u$. As a result, the local reconstruction operator R_K^k can be defined by solving the following approximation problem: to find $R_K^k u \in Q^k(S(K))$ such that

$$I_{K_\theta}^\alpha R_K^k u = I_{K_\theta}^\alpha u, \quad \forall K_\theta \in S(K), \quad \alpha \in A^m, \quad m < k. \quad (3.5)$$

Given the stencil, we can make sure the system (3.5) is determined by increasing the order of Legendre moments, m . In the next section, we will discuss in detail the relation of m and k and give the well-posedness of the defined reconstruction operator. The proposal of this reconstruction operator, which requires only a narrow stencil, is one of the main contributions of this paper.

After that, the global reconstruction operator $R^k : V_h^m \rightarrow V_h^k$ is naturally defined piecewise: let the restriction of global approximation $R^k u$ be the corresponding local approximation $R_K^k u$, i.e.,

$$(R^k u)|_K = R_K^k u, \quad \forall K \in \mathcal{T}_h. \quad (3.6)$$

We can observe that the global reconstruction operator R^k embeds the piecewise polynomial space V_h^m into a higher order piecewise polynomial V_h^k . Let the embedded space be denoted by $U_h^k = R^k V_h^m$.

3.2 Properties for the reconstruction operator

For a better application of the reconstruction operator R^k , we would like to analyze its properties. Let us begin with a problem left over from the last section: the well-posedness of the local reconstruction operator R_K^k . It is equivalent to the existence and uniqueness of the solutions for the approximation problem (3.5), which can be deduced from the following assumption directly.

Assumption 1. *For every $K \in \mathcal{T}_h$ and $w \in Q^k(S(K))$, if the Legendre moments satisfy that*

$$I_{K_\theta}^\alpha w = 0, \quad \forall K_\theta \in S(K), \quad \alpha \in A^m, \quad (3.7)$$

we must have $w|_{S(K)} \equiv 0$.

For the cases of $k = 2, 5$, the detailed numerical analysis is presented in Appendix A. We can observe that Assumption 1 holds when satisfying $(k + 1)/(m + 1) = 3$, where 3 is the width of the stencil. For instance, the reconstruction operator R_K^5 demands a set of Legendre moments $\{I_{K_\theta}^\alpha u\}$ with $\alpha \in A^1$ and $K_\theta \in S(K)$. In the following sections, we call the relation $(k + 1)/(m + 1) = 3$ well-posed condition. Remark that the same condition is expected to be derived for the higher-order cases.

Under Assumption 1, we can define a kind of l_∞ norm for any $u \in Q^k(S(K))$ based on the Legendre moments as follows,

$$\|u\|_{l_\infty(S(K))} = \max_{K_\theta \in S(K), \alpha \in A^m} |I_{K_\theta}^\alpha u|.$$

On one side, the equivalence of the norms over finite dimensional space $Q^k(S(K))$ leads to the following property

$$\|u\|_{0,\infty,S(K)} \leq C \|u\|_{l_\infty(S(K))}, \quad \forall u \in Q^k(S(K)). \quad (3.8)$$

On the other side, based on the boundedness of Legendre functions $L_{K_\theta}^\alpha$, we can find an upper bound C such that

$$\max_{K_\theta \in S(K), \alpha \in A^m} |I_{K_\theta}^\alpha 1| \leq C.$$

Therefore, for any $u \in C^0(S(K))$, we have

$$\|u\|_{l_\infty(S(K))} \leq C \|u\|_{0,\infty,S(K)}. \quad (3.9)$$

With the help of this norm, in Appendix B, we provide the proof of the following theorem where the approximation properties of the local reconstruction operator are presented.

Theorem 1. *If Assumption 1 holds, the k -exactness property holds for any $K \in \mathcal{T}_h$ as*

$$R_K^k u = u, \quad \forall u \in Q^k(S(K_j)). \quad (3.10)$$

Moreover, for any $K \in \mathcal{T}_h$ the local approximation $R_K^k u$ with $u \in H^{k+1}(S(K))$ satisfies the L^∞ error estimate as

$$\|u - R_K^k u\|_{0,\infty,K} \leq Ch^{k+1-\frac{d}{2}}, \quad (3.11)$$

and the L^2 error estimate holds as follows

$$\|u - R_K^k u\|_{0,K} \leq Ch^{k+1}, \quad (3.12)$$

$$|u - R_K^k u|_{1,K} \leq Ch^k, \quad (3.13)$$

where C depends on $|u|_{H^{k+1}(S(K))}$ but is independent of h .

3.3 The reduced discontinuous Galerkin space

In this subsection, we would like to further explore the approximation space U_h^k . For all $K \in \mathcal{T}_h, \alpha \in A^m$, consider the following locally supported functions defined on the domain Ω

$$v_K^\alpha = \begin{cases} L_K^\alpha(\mathbf{x}), & \mathbf{x} \in K, \\ 0, & \text{elsewhere.} \end{cases} \quad (3.14)$$

They span the piecewise polynomial space V_h^m completely. By applying the reconstruction operator R^k on each function v_K^α , we can define the basis function of space U_h^k by

$$\phi_K^\alpha = R^k v_K^\alpha. \quad (3.15)$$

Therefore, any approximation function $R^k u \in U_h^k$ can be expressed by the basis expansion:

$$R^k u = \sum_{K \in \mathcal{T}_h, \alpha \in A^m} (I_K^\alpha u) \phi_K^\alpha.$$

By the definitions (3.6), (3.14), and (3.15), we know that the basis function ϕ_K^α belongs to the piecewise polynomial space V_h^k and has a compactly supported set $S(K)$. With the relation of m and k introduced in Section 3.2, we can conclude that the space U_h^k of cardinality $N(m+1)^d$ certainly is the subspace of the general piecewise polynomial space V_h^k and the reduction of $1/3^d$ degree of freedom can be appreciated. According to [17], the number of DoFs can be regarded as a proper indicator of the efficiency in a specific discrete system. From this point of view, the DG methods based on the RDG space can achieve higher efficiency. Moreover, our narrow-stencil reconstruction method ensures the local property of these basis functions, which prevents the local property of DG approaches from being destroyed.

Up to this point, we have defined an approximation space U_h^k with reduced cardinality but the same accuracy as the standard DG space V_h^k , called the reduced discontinuous Galerkin (RDG) space. Considering the above properties of the RDG space, it is easy to implement various DG methods with our RDG space.

4 The LDG method with the RDG space

4.1 The semi-discrete LDG scheme

Here, we only focus on the periodic boundary condition for simplicity. Notice that the analysis can be extended to other non-periodic boundary conditions [28]. It is worth noting that the RDG space is not limited to the LDG method, but can be applied to other DG methods as well.

To describe the LDG method, we begin with the following first-order system equivalent to the CDR equation (1.1a):

$$\begin{cases} u_t + \nabla \cdot (\mathbf{b}(\mathbf{x})f(u) - \sqrt{\varepsilon}\mathbf{q}) + r(u) = g(\mathbf{x}, t), \\ \mathbf{q} = \sqrt{\varepsilon}\nabla u. \end{cases}$$

Given the rectangular mesh \mathcal{T}_h , the functions in the RDG space are piecewise continuous, whose behavior on the set of edges \mathcal{E}_h may be undefined. Here we introduce some definitions to handle this case. Let $e \in \mathcal{E}_h$ be the edge of any element $K \in \mathcal{T}_h$. For a scalar function $u_h \in U_h^k$, we denote its two traces on e along the positive and negative direction of the coordinate axis by u_h^+ and u_h^- . The jump and the mean of function u_h at edge e are denoted by $[u_h] = u_h^+ - u_h^-$ and $\bar{u}_h = \frac{1}{2}(u_h^+ + u_h^-)$. We denote by \mathbf{n}^+ the unit normal at e of K along the positive direction of the coordinate axis and denote by \mathbf{n}^- its reverse. For a vector function $\mathbf{u}_h \in (U_h^k)^d$, the jump of it is denoted by $[\mathbf{u}_h] = \mathbf{u}_h^+ \cdot \mathbf{n}^+ + \mathbf{u}_h^- \cdot \mathbf{n}^-$. Let $\mathbf{n} = (n_1, \dots, n_d)$ denote the unit outward normal on the boundary ∂K , and $(\cdot, \cdot)_K$ and $\langle \cdot, \cdot \rangle_{\partial K}$ denote the inner product on element K and boundary ∂K respectively.

The semi-discrete LDG scheme can be defined: find $u_h \in U_h^k$ and $\mathbf{q}_h = (q_h^1, \dots, q_h^d) \in (U_h^k)^d$ such that, for any $t > 0$ and $K \in \mathcal{T}_h$, we have

$$\begin{cases} ((u_h)_t, v_h)_K = \mathcal{H}_K(u_h, v_h) + \mathcal{L}_K(\mathbf{q}_h, v_h) + \mathcal{R}_K(u_h, v_h) + \mathcal{G}_K(\mathbf{x}, t, v_h), \quad \forall v_h \in U_h^k, \\ (q_h^i, p_h^i)_K = \mathcal{K}_K^i(u_h, p_h^i), \quad \forall p_h^i \in U_h^k, \quad i = 1, \dots, d. \end{cases} \quad (4.16)$$

Here, all operators in the above weak formulation are defined as follows,

$$\mathcal{H}_K(u_h, v_h) = \left((\mathbf{b}(\mathbf{x})f(u_h), \nabla v_h)_K - \langle \mathbf{b}(\mathbf{x})\hat{f}(u_h) \cdot \mathbf{n}, v_h \rangle_{\partial K} \right), \quad (4.17a)$$

$$\mathcal{L}_K(\mathbf{q}_h, v_h) = -\sqrt{\varepsilon} \left((\mathbf{q}_h, \nabla v_h)_K - \langle \hat{\mathbf{q}}_h \cdot \mathbf{n}, v_h \rangle_{\partial K} \right), \quad (4.17b)$$

$$\mathcal{K}_K^i(u_h, p_h^i) = -\sqrt{\varepsilon} \left((u_h, (p_h^i)_{x_i})_K - \langle \hat{u}_h, p_h^i n_i \rangle_{\partial K} \right), \quad (4.17c)$$

$$\mathcal{R}_K(u_h, v_h) = -(r(u_h), v_h)_K, \quad (4.17d)$$

$$\mathcal{G}_K(\mathbf{x}, t, v_h) = (g(\mathbf{x}, t), v_h)_K, \quad (4.17e)$$

where $\hat{f}(u_h)$, $\hat{\mathbf{q}}_h$, and \hat{u}_h are the boundary terms, which are called numerical flux. To guarantee stability, they need specific designs with the two-sided traces on the boundary. Following the choice strategy described in [11, 29], we take the monotone flux for the convection part and the alternating flux for the diffusion part, defined as

$$\hat{f}(u_h) = \hat{f}(u_h^-, u_h^+), \quad \hat{\mathbf{q}}_h = \mathbf{q}_h^+, \quad \hat{u}_h = u_h^-.$$

Note that there are several well-known examples of monotone fluxes $\hat{f}(u_h^-, u_h^+)$, such as the Lax-Friedrichs flux, Godunov flux, and Engquist-Osher flux, etc [10]. For the convenience of error analysis, the numerical flux can be written in the following viscosity form

$$\hat{f}(u_h^-, u_h^+) = \frac{1}{2} \left(f(u_h^-) + f(u_h^+) - \alpha(u_h^-, u_h^+)(u_h^+ - u_h^-) \right),$$

with the assumption $\alpha(u_h^-, u_h^+) \geq \alpha_0$ where α_0 is a positive number.

Here we denote the global inner product by

$$(u, v) = \sum_{K \in \mathcal{T}_h} (u, v)_K, \quad \langle u, v \rangle = \sum_{e \in \mathcal{E}_h} \langle u, v \rangle_e.$$

By summing up the equation (4.16) over $K \in \mathcal{T}_h$, we obtain the global weak formulation, as follows,

$$\begin{cases} ((u_h)_t, v_h) = \mathcal{H}(u_h, v_h) + \mathcal{L}(\mathbf{q}_h, v_h) + \mathcal{R}(u_h, v_h) + \mathcal{G}(\mathbf{x}, t, v_h), \quad \forall v_h \in U_h^k, \\ (q_h^i, p_h^i) = \mathcal{K}^i(u_h, p_h^i), \quad \forall p_h^i \in U_h^k, \quad i = 1, \dots, d, \end{cases} \quad (4.18)$$

where \mathcal{H} , \mathcal{L} , \mathcal{R} , \mathcal{G} , \mathcal{K}^i are the global operators defined by summing up the corresponding local operators of formulation (4.17) over all elements $K \in \mathcal{T}_h$.

4.2 Error estimate for the semi-discrete LDG scheme

The properties in this subsection are the direct extension results in [29] where we refer the readers for more details. Given the mesh \mathcal{T}_h , we first introduce the broken energy space

$$W^{s,p}(\mathcal{T}_h) = \{v \in L^2(\Omega) : v|_K \in W^{s,p}(K), \forall K \in \mathcal{T}_h\},$$

and denote the corresponding seminorm and norm by

$$|v|_{s,p} = \left(\sum_{K \in \mathcal{T}_h} |v|_{s,p,K}^p \right)^{\frac{1}{p}}, \quad \|v\|_{s,p} = \left(\sum_{j=1}^N |v|_{s,p}^p \right)^{\frac{1}{p}}.$$

For $p = 2$, we omit the index p and simply denote these norms by $|v|_s$, and $\|v\|_s$. Similarly, we can denote the broken energy space on the boundary set by $W^{s,p}(\mathcal{E}_h)$ and its norms by $|v|_{s,p,\mathcal{E}_h}$ and $\|v\|_{s,p,\mathcal{E}_h}$.

With the above global notation, we present the approximation properties for the global reconstruction operator R^k as follows,

Theorem 2. *Let $u \in H^{k+1}(\Omega)$, the global approximation $R^k u$ satisfies the following error estimates*

$$\|u - R^k u\|_0 \leq Ch^{k+1}, \quad (4.19)$$

$$|u - R^k u|_1 \leq Ch^k. \quad (4.20)$$

$$\|u - R^k u\|_0 + h^{\frac{d}{2}} \|u - R^k u\|_{0,\infty} + h^{\frac{1}{2}} \|u - R^k u\|_{0,\mathcal{E}_h} \leq Ch^{k+1}. \quad (4.21)$$

Proof. By summing up all elements, properties (4.19) and (4.20) can be derived by the Theorem 1 directly. Together with Theorem 1 and the Agmon inequality (2.2), the property (4.21) can be derived. \square

Now, we introduce the error estimate for the semi-discrete LDG scheme. The detailed proof is provided in Appendix C.

Theorem 3. *Let $u \in H^{k+1}(\Omega)$ be the exact solution of equation (1.1), and $u_h \in U_h^k$ be the numerical solution of scheme (4.18). Then for small enough h , there exists C such that*

$$\|u - u_h\|_0 \leq Ch^k, \quad (4.22)$$

where C depends on the final time T , k , $\|u\|_{H^{k+1}}$, $\|\mathbf{b}\|_{1,\infty}$, $|\varepsilon|$ and the upper bound of $|f^{(m)}|$ for $m = 1, 2, 3$.

Remark 1. *The proof of Theorem 3 follows [29] where the author presented the results for the one- and two-dimensional cases and the $(k + \frac{1}{2})$ th order L^2 norm estimate was given. Here, we can only obtain the k th order L^2 norm estimate in theory, although the $(k + 1)$ th order convergence results can be observed numerically in Section 5.1. The main problem is that there are not enough DoFs for us to define some kind of L^2 -projection with multiple orthogonal properties which always plays an important role in eliminating the order-reduction terms during error estimates, such as the jump terms and the partial terms [7].*

4.3 Fully discrete IMEX RK LDG scheme

In this section, we would like to introduce the third-order IMEX RK method [6] for time discretization, which treats the nonlinear terms, such as convection, reaction, and source terms explicitly but the linear diffusion term implicitly. It is a kind of balanced scheme which does not subject to severe time step restriction while avoiding large nonlinear system solver. The simplicity and good performance of this method make it famous among many others, although the choice of implicit parts is too rough to handle the case of very stiff reaction terms. For the IMEX RK method coupled with the semi-discrete LDG scheme for solving convection-diffusion problems, Wang et al. have proposed a much weaker stability condition $\Delta t \leq C$ with a constant C , where Δt is the time step [26]. However, here we only consider a standard CFL stability condition $\Delta t \leq Ch$ for our nonlinear CDR equation.

To describe the IMEX RK method distinctly, we consider the system (4.18) as the following simple ordinary differential equation (ODE) form

$$\begin{aligned}\frac{dU(t)}{dt} &= L^1(t, \mathbf{Q}) + N(t, U), \\ \mathbf{Q} &= L^2(t, U), \\ U(0) &= U^0,\end{aligned}$$

where U is the undetermined coefficient vector, $L^1(t, \mathbf{Q})$ and $L^2(t, U)$ represent the linear diffusion part, $N(t, U)$ represents the nonlinear part, such as convection, reaction, and force part, in semi-discrete LDG scheme. Let U^n be the numerical approximation at time t^n . One step time evolution of the three-stage third-order IMEX RK scheme is given by

$$\begin{aligned}U^{(1)} &= U^n, \\ U^{(i)} &= U^n + \Delta t \sum_{j=2}^i a_{ij} L^1(t_j^n, \mathbf{Q}^{(j)}) + \Delta t \sum_{j=1}^{i-1} \hat{a}_{ij} N(t_j^n, U^{(j)}), \quad 2 \leq i \leq 4, \\ U^{n+1} &= U^n + \Delta t \sum_{i=2}^4 b_i L^1(t_i^n, \mathbf{Q}^{(i)}) + \Delta t \sum_{i=1}^4 \hat{b}_i N(t_i^n, U^{(i)}), \\ \mathbf{Q}^{(i)} &= L^2(t_i^n, U^{(i)}), \quad 2 \leq i \leq 4.\end{aligned}\tag{4.23}$$

Where $U^{(i)}$ denotes the intermediate stages at the corresponding time $t_i^n = t^n + c_i \Delta t$. All the coefficients in the scheme are presented in the following Butcher tableau

$$\begin{array}{c|cc} \mathbf{c} & A & \hat{A} \\ \hline & \mathbf{b}^T & \hat{\mathbf{b}}^T \end{array}$$

which is specified as follows,

0	0	0	0	0	0	0	0	0
γ	0	γ	0	0	γ	0	0	0
$\frac{1+\gamma}{2}$	0	$\frac{1-\gamma}{2}$	γ	0	$\frac{1+\gamma}{2} - \alpha_1$	α	0	0
1	0	β_1	β_2	γ	0	$1-\alpha_2$	α_2	0
	0	β_1	β_2	γ	0	β_1	β_2	γ

where the parameters are selected as $\gamma \approx 0.435866521508459$, $\beta_1 = -\frac{3}{2}\gamma^2 + 4\gamma - \frac{1}{4}$, $\beta_2 = \frac{3}{2}\gamma^2 - 5\gamma - \frac{5}{4}$, $\alpha_1 = -0.35$, and $\alpha_2 = \frac{\frac{1}{3}-2\gamma^2-2\beta_2\alpha_1\gamma}{\gamma(1-\gamma)}$ [6].

So far, we have developed the fully discrete IMEX RK LDG scheme by combining the semi-discrete LDG scheme (4.18) and the IMEX RK scheme (4.23). In this type of scheme, repetitively solving large linear systems is the main challenge for the computation cost. This allows the full benefit of RDG space to be realized in terms of cost savings.

5 Numerical examples

In this section, we would like to validate our scheme and study its numerical behavior. The numerical results focus mainly on the following aspects: First, we demonstrate the convergence behavior of the third-and sixth-order IMEX RK LDG scheme proposed based on the RDG space. Secondly, we investigate the ability to capture sharp layers for our method, which demonstrates the local property of our reconstruction operator.

5.1 Convergence order study

1D-Test 1 Consider the linear convection-diffusion equation

$$u_t + u_x - u_{xx} = g(t, x), \quad x \in [0, 2\pi].$$

1D-Test 2 Consider the nonlinear convection-diffusion equation

$$u_t + \left(\frac{u^2}{2}\right)_x - u_{xx} = g(t, x), \quad x \in [-\pi, \pi].$$

The same initial condition $u(x, 0) = \sin(x)$ and periodic boundary condition are used for the above two tests. Moreover, the same exact solution is given by $u(x, t) = \sin(x - t)$. Then the right-hand sides of these two tests can be obtained by a simple calculation.

1D-Test 3 We seek traveling wave solutions for the equation

$$u_t - \nu^2 u_{xx} + u^3 - u = 0, \quad x \in [-1, 1],$$

$$u(x, 0) = \frac{1}{2} \left(1 - \tanh\left(\frac{x}{2\sqrt{2\nu}}\right)\right).$$

The Dirichlet boundary condition is given by the exact solution $u(x, t) = \frac{1}{2} \left(1 - \tanh\left(\frac{x-st}{2\sqrt{2\nu}}\right)\right)$, where $s = 3\nu/\sqrt{2}$ is the speed of the traveling wave. Here, the value of the diffusion velocity is $\nu^2 = 0.01$.

2D-Test 1 Consider linear convection diffusion equation

$$u_t + \nabla \cdot u - \Delta u = g(t, x, y), \quad x, y \in [0, 2\pi] \times [0, 2\pi].$$

2D-Test 2 Consider nonlinear convection diffusion equation

$$u_t + \nabla \cdot \left(\frac{u^2}{2}\right) - \Delta u = g(t, x, y), \quad x, y \in [0, 2\pi] \times [0, 2\pi].$$

For the 2D-Test1 and 2D-Test2, let $u(x, y, t) = \sin(x + y - 2t)$ be the exact solution. Naturally, the initial value conditions and the right-hand sides of these two tests are given. Here we consider the periodic boundary condition.

2D-Test 3 Consider the Allen-Cahn equation

$$u_t - \Delta u + \frac{1}{\nu^2}(u^3 - u) = g(t, x, y), \quad x, y \in [0, 2\pi] \times [0, 2\pi],$$

with the initial value $u(x, y, 0) = \sin(x + y)$ and the periodic boundary condition. Here, $\nu = 0.3$. The source term $g(x, y, t)$ is given by the exact solution $u(x, y, t) = \exp(-2t) \sin(x + y)$.

With the terminal time $t = 1$ and the fixed CFL condition $\Delta t = h$, we apply the third- and sixth-order IMEX RK LDG scheme with the RDG space (i.e. $k = 2, 5$) for solving 1D-Test1 to 3 on a series of meshes with the number of the elements $N = 2^4, 2^5, 2^6, \dots, 2^9$. The L^2 -norm errors in approximation to the exact solution u and its first derivative u_x are presented in Figure 5.1. We can observe that both the error $\|u - u_h\|_{L^2}$ and the error $\|u_x - q_h\|_{L^2}$ converge at the optimal rate $O(h^{k+1})$ for these tests. For two dimensions, let the CFL number be 0.5 for 2D-Test 1 and 2D-Test 2, and 0.2 for 2D-Test 3. Here, we consider the uniform rectangular meshes with the number of the elements $N = 20^2, 30^2, 40^2, \dots, 70^2$ for the computation. We also compute the errors at $t = 1$. Figure 5.2 demonstrates the results which show the same conclusion as the one-dimensional case.

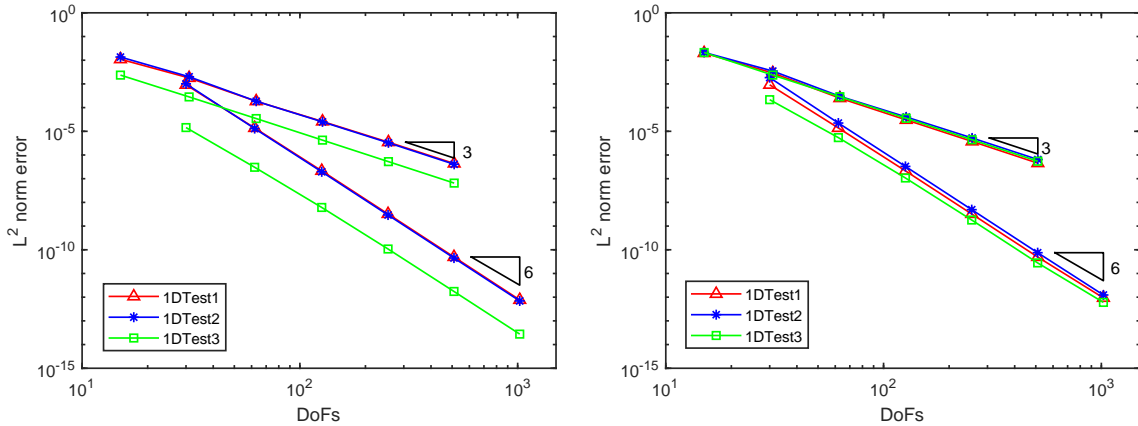


Figure 5.1: The convergence rates of $\|u - u_h\|_{L^2(\mathcal{T}_h)}$ (left) and $\|u_x - q_h\|_{L^2(\mathcal{T}_h)}$ (right).

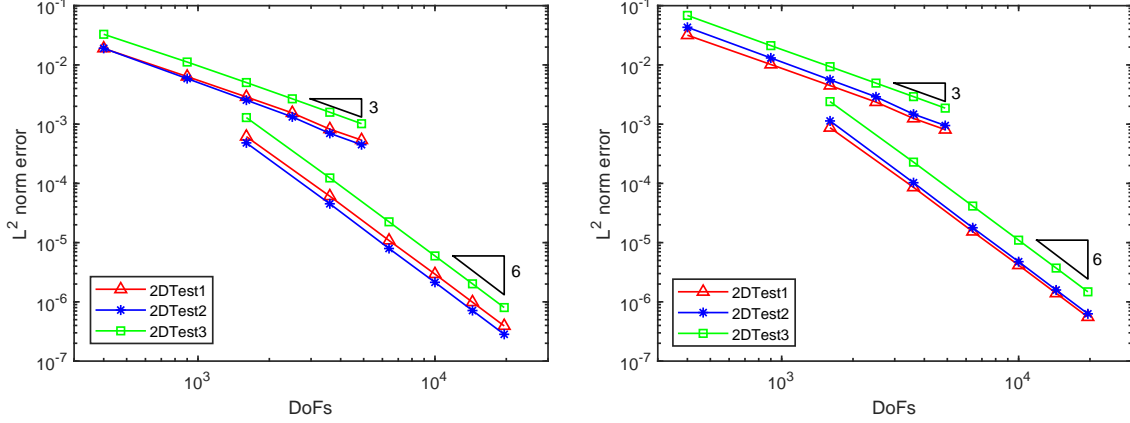


Figure 5.2: The convergence rates of $\|u - u_h\|_{L^2(\mathcal{T}_h)}$ (left) and $\|\nabla u - \mathbf{q}_h\|_{L^2(\mathcal{T}_h)}$ (right).

5.2 Local property verification

1D-Test 4 Consider the viscous Burgers equation with the Dirichlet boundary condition

$$u_t + \left(\frac{u^2}{2}\right)_x - \nu u_{xx} + \pi \cos(\pi x)u = 0, \quad x \in [0, 1],$$

$$u(0, t) = 1, \quad u(1, t) = -0.1.$$

The initial condition is given as follows,

$$u(x, 0) = \begin{cases} 1, & 0 \leq x \leq 0.3, \\ -0.1, & 0.3 < x \leq 1. \end{cases}$$

2D-Test 4 Consider the viscous Burgers problem in [21]

$$u_t + \nabla \cdot \left(\frac{u^2}{2}\right) - \nu \Delta u = g(x, y, t), \quad x, y \in [0, 1] \times [0, 1],$$

with the homogeneous Dirichlet boundary condition and the initial condition $u(x, y, 0) = 0$. The source term $g(x, y, t)$ is given by the exact solution $u(x, y, t) = (\exp(t) - 1)xy \tanh(\frac{1-x}{\nu}) \tanh(\frac{1-y}{\nu})$.

2D-Test 5 Consider the rigid body rotation problem

$$u_t + \nabla \cdot (\boldsymbol{\alpha}(x, y)u) - \nu \Delta u = 0, \quad x, y \in [-2\pi, 2\pi] \times [-2\pi, 2\pi],$$

where $\boldsymbol{\alpha}(x, y) = (-y, x)^T$. Here we consider the same boundary condition as 2D-Test 4. Following [14, Example 3.4], the initial condition includes a slotted disk, a cone, and a smooth hump.

We take the diffusion viscosity coefficients $\nu = 10^{-3}$ for 1D-Test4 and 2D-Test5, and $\nu = 10^{-2}$ for 2D-Test4. For 2D-Test 4, we have a representation of the exact solution. For 1D-Test 4 and 2D-Test 5, without the exact solutions, let the numerical solutions solved on the fine meshes be regarded as the surrogate exact solutions. In Figure 5.3, we

present these exact solutions at $t = 1$. We can find that there are layers near $x = 0.5$, along $x = 0$ and $y = 1$, and on the boundary of a slotted disk for the solutions of 1D-Test 4, 2D-Test4, and 2D-Test 5 respectively. Note that the position of the layer for 2D-Test 5 moves in a counterclockwise direction with time, which is challenging for numerical simulation.

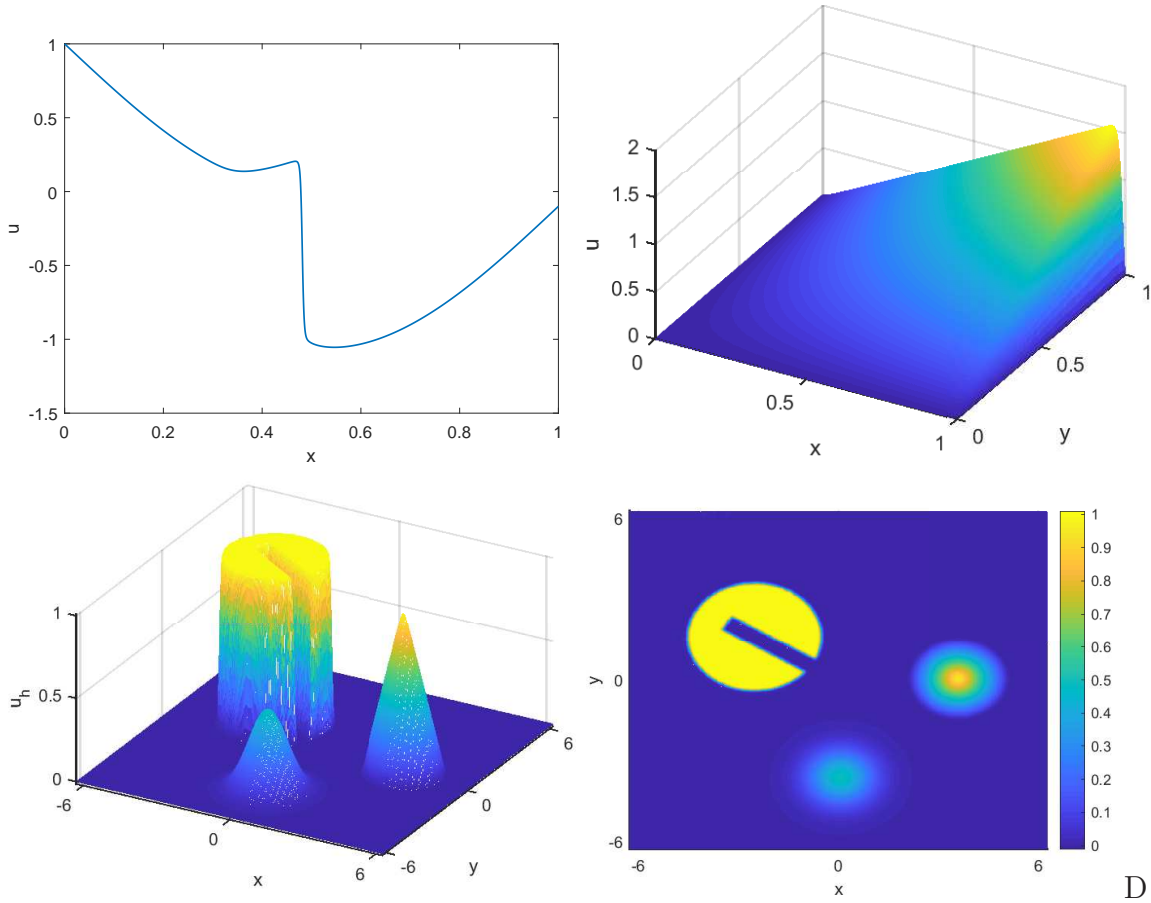


Figure 5.3: The image of the (surrogate) exact solutions for 1D-Test 4 (Left Top), 2D-Test 4 (Right Top), and 2D-Test 5 (Left Bottom). And the overlooking 2D image for 2D-Test 5 (Right Bottom).

We apply the third- and sixth-order methods proposed in this article to solve the above three tests with different numbers of elements N . The plots of the numerical solutions are presented in Figure 5.4-5.6. We can observe that, when coarse mesh, there is some overshooting/undershooting near the layer or the region where the layer goes through along with the time. As the mesh is refined, the overshooting/undershooting becomes smaller and smaller until the layers can be well captured. Under the same mesh size, the higher-order method shows more excellent performance in capturing the layer. This is not only because of its intrinsically higher approximation accuracy but also as the fixed narrow stencil applied in our method guarantees the local data structure property for different order methods.

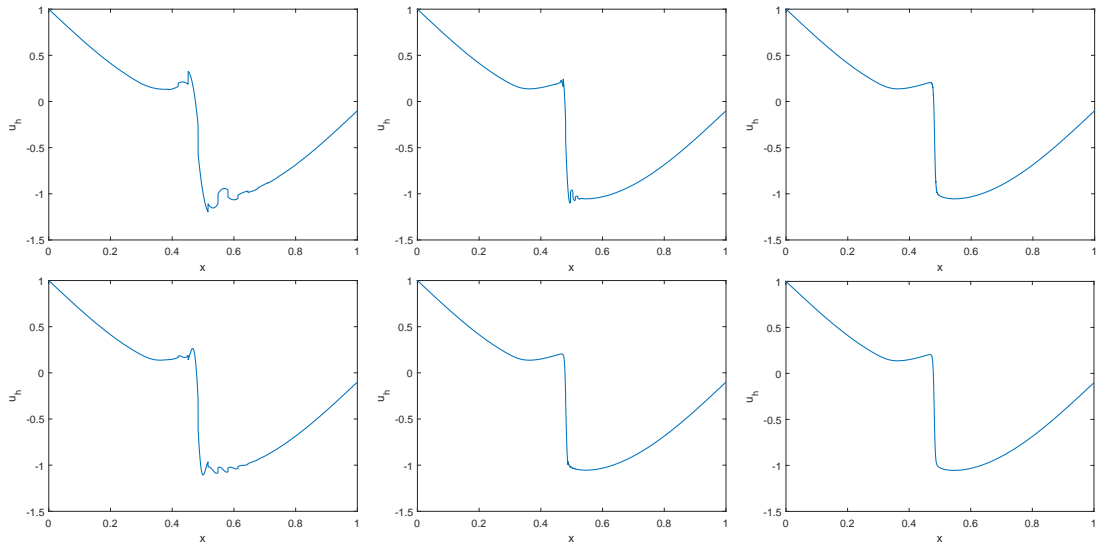


Figure 5.4: The image of the numerical solutions for 1D-Test 4. Top row: numerical solutions for the third-order method with $N = 32, 128, 512$ (from Left to Right). Bottom row: numerical solutions for the sixth-order method.

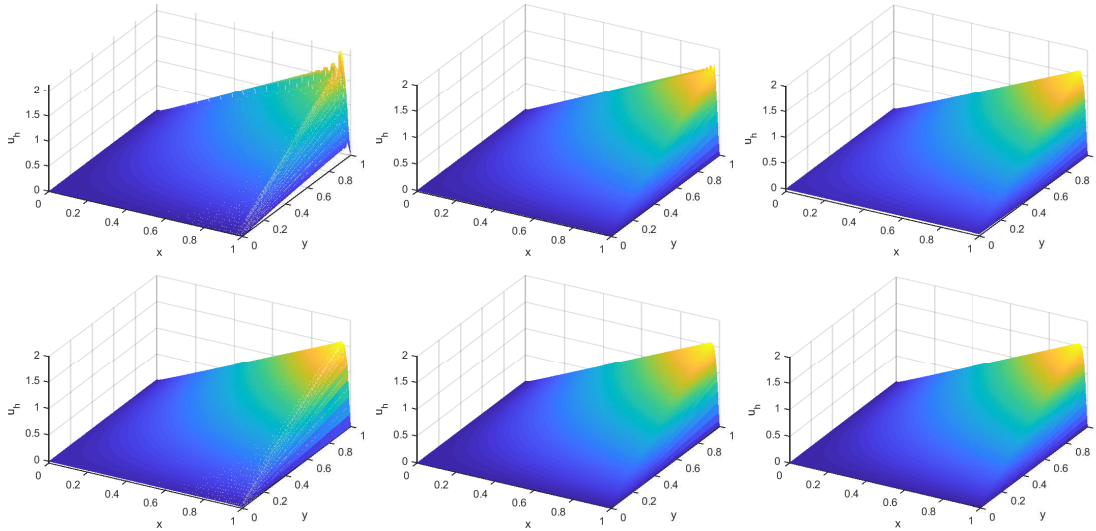


Figure 5.5: The image of the numerical solutions for 2D-Test 4. Top row: numerical solutions for the third-order method with $N = 50^2, 100^2, 150^2$ (from Left to Right). Bottom row: numerical solutions for the sixth-order method.

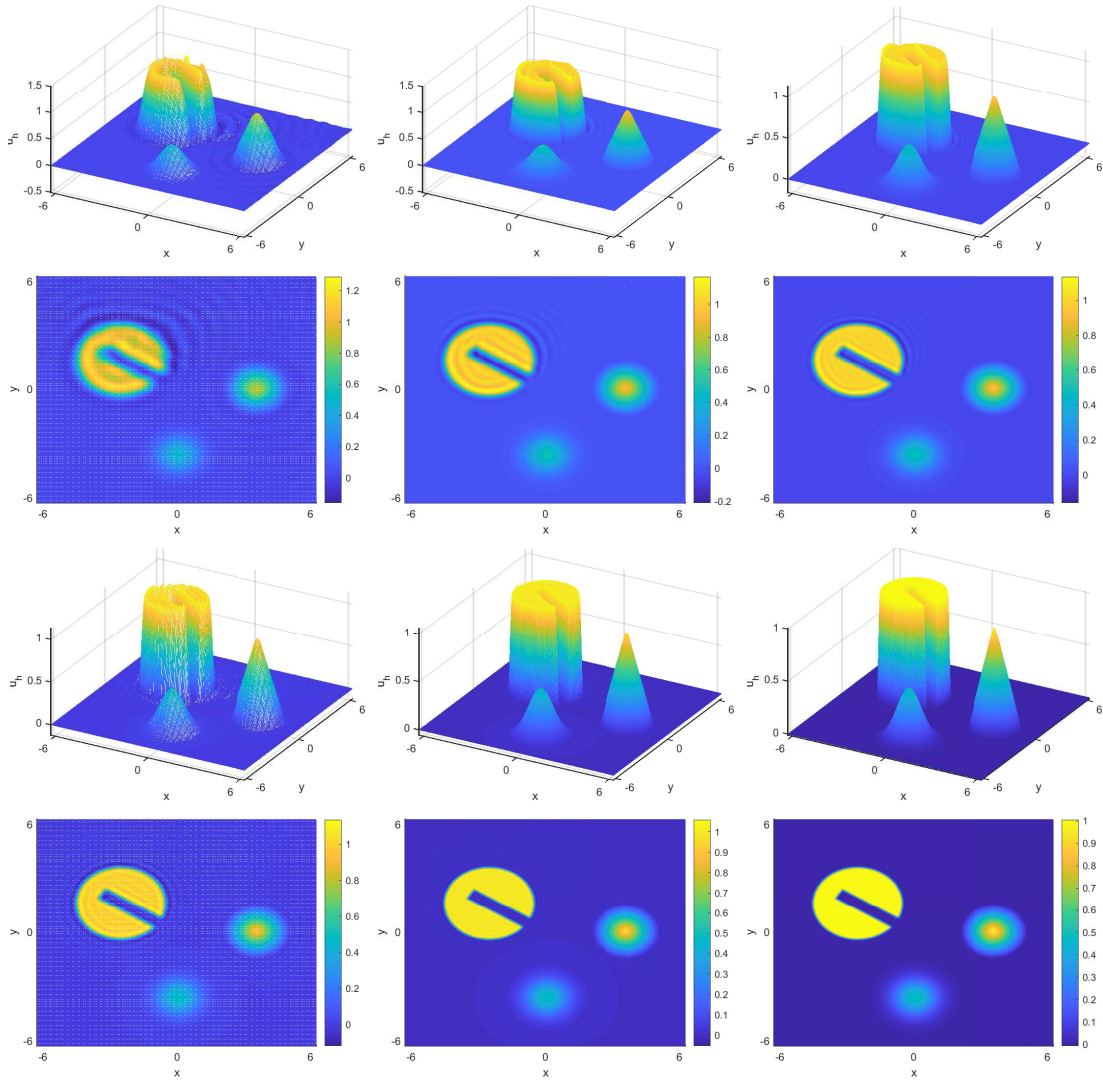


Figure 5.6: The 3D and overlooking 2D image of the numerical solutions for 2D-Test 5. Top two rows: numerical solutions for the third-order method with $N = 50^2, 100^2, 150^2$ (from Left to Right). Bottom two rows: numerical solutions for the sixth-order method.

6 Conclusion

In this paper, we have constructed the RDG space, which has the same order of accuracy as the standard DG space but uses fewer DoFs, where a narrow stencil reconstruction approach is proposed by using the high-order Legendre moments with the aim of maintaining the local property for the DG methods. Based on this approximation space, we apply the IMEX RK LDG method to the nonlinear CDR equation and present the error estimate in the L^2 norm. Several numerical experiments are presented to demonstrate the accuracy and performance of our method. The same idea can be applied to the irregular domain and partitions in our ongoing work.

A The numerical analysis of Assumption 1

Without loss of generality, consider any element $K_\theta \in \mathcal{T}_h$. The stencil of K_θ introduced in Section 3.1 is written as $S^d(K_\theta) = \{K_{\theta^1}, K_{\theta^2}, \dots, K_{\theta^s}\}$, where $s = 3^d$ is the number of elements in the stencil. For convenience, we define the trace of a multiple indicator $\alpha = (\alpha_1, \dots, \alpha_n)$ by $tr(\alpha) = \sum_{i=1}^n \alpha_i$ and sort the set A^k based on the ascendant sequence of the trace, i.e.,

$$A^k = \{\alpha^1, \alpha^2, \dots, \alpha^{(k+1)^d}\},$$

where $tr(\alpha^1) \leq tr(\alpha^2) \leq \dots \leq tr(\alpha^{(k+1)^d})$.

As a result, we can express the approximation $R_{K_\theta}^k u$ as the following Legendre expansion

$$R_{K_\theta}^k u(\mathbf{x}) = \sum_{j=1}^{(k+1)^d} u^{\alpha^j} L_{K_\theta}^{\alpha^j}(\mathbf{x}),$$

where $\mathbf{u} = (u^{\alpha^1}, u^{\alpha^2}, \dots, u^{\alpha^{(k+1)^d}})^T$ is the unknown coefficient vector to be determined.

For any element $K_{\theta^i} \in S^d(K_\theta)$, let $M_{K_{\theta^i}}^k$ denote an $(m+1)^d \times (k+1)^d$ matrix whose j th row is the Legendre moments vector obtained by applying the operator $I_{K_{\theta^i}}^{\alpha^j}$ on the Legendre basis vector $(L_{K_\theta}^{\alpha^1}(\mathbf{x}), L_{K_\theta}^{\alpha^2}(\mathbf{x}), \dots, L_{K_\theta}^{\alpha^{(k+1)^d}}(\mathbf{x}))$, i.e.,

$$m_{K_{\theta^i}}^k = \begin{pmatrix} I_{K_{\theta^i}}^{\alpha^1} L_{K_\theta}^{\alpha^1}(\mathbf{x}) & I_{K_{\theta^i}}^{\alpha^1} L_{K_\theta}^{\alpha^2}(\mathbf{x}) & \dots & I_{K_{\theta^i}}^{\alpha^1} L_{K_\theta}^{\alpha^{(k+1)^d}}(\mathbf{x}) \\ I_{K_{\theta^i}}^{\alpha^2} L_{K_\theta}^{\alpha^1}(\mathbf{x}) & I_{K_{\theta^i}}^{\alpha^2} L_{K_\theta}^{\alpha^2}(\mathbf{x}) & \dots & I_{K_{\theta^i}}^{\alpha^2} L_{K_\theta}^{\alpha^{(k+1)^d}}(\mathbf{x}) \\ \vdots & \vdots & & \vdots \\ I_{K_{\theta^i}}^{\alpha^{(m+1)^d}} L_{K_\theta}^{\alpha^1}(\mathbf{x}) & I_{K_{\theta^i}}^{\alpha^{(m+1)^d}} L_{K_\theta}^{\alpha^2}(\mathbf{x}) & \dots & I_{K_{\theta^i}}^{\alpha^{(m+1)^d}} L_{K_\theta}^{\alpha^{(k+1)^d}}(\mathbf{x}) \end{pmatrix}.$$

Repeating the same process for every elements of the stencil $S^d(K_\theta)$, we can define the coefficient matrix of the linear system (3.7) by

$$M_{K_\theta}^k = \left(m_{K_{\theta^1}}^T, m_{K_{\theta^2}}^T, \dots, m_{K_{\theta^s}}^T \right)^T. \quad (\text{A.1})$$

Ultimately, we obtain the matrix version of the system (3.7) as follows:

$$M_{K_\theta}^k \mathbf{u} = \mathbf{0}, \quad (\text{A.2})$$

where $\mathbf{0}$ is the zeros vector.

For this system to have unique zero solution, there are two conditions to be simultaneously satisfied:

1. Matrix $M_{K_\theta}^k$ is a square matrix, i.e., $(k+1)/(m+1) = 3$.
2. The determinant of matrix $M_{K_\theta}^k$ must be non-zero.

Under the first condition, let us discuss the second condition. To do that, we need to figure out each element of $M_{K_\theta}^k$. Take the element $I_{K_{\theta i}}^{\alpha^r} L_{K_\theta}^{\alpha^l}(\mathbf{x})$ for example, we have

$$\begin{aligned}
I_{K_{\theta i}}^{\alpha^r} L_{K_\theta}^{\alpha^l}(\mathbf{x}) &= \left(\prod_{j=1}^d \frac{2\alpha_j^r + 1}{h_{K_{\theta i}}^j} \right) \int_{K_{\theta i}} L_{K_{\theta i}}^{\alpha^r}(\mathbf{x}) L_{K_\theta}^{\alpha^l}(\mathbf{x}) d\mathbf{x} \\
&= \prod_{j=1}^d \left(\frac{2\alpha_j^r + 1}{2} \int_{-1}^1 \widehat{L}^{\alpha_j^r}(\widehat{x}) L_{K_\theta}^{\alpha_j^l} \left(\frac{h_{K_{\theta i}}^j}{2} \widehat{x} + x_{K_{\theta i}}^j \right) d\widehat{x} \right) \\
&= \prod_{j=1}^d \left(\frac{2\alpha_j^r + 1}{2} \int_{-1}^1 \widehat{L}^{\alpha_j^r}(\widehat{x}) \widehat{L}^{\alpha_j^l} \left(\frac{h_{K_{\theta i}}^j}{h_{K_\theta}^j} \widehat{x} + \frac{2}{h_{K_\theta}^j} (x_{K_{\theta i}}^j - x_{K_\theta}^j) \right) d\widehat{x} \right) \\
&= \prod_{j=1}^d \left(\frac{2\alpha_j^r + 1}{2} \int_{-1}^1 \widehat{L}^{\alpha_j^r}(\widehat{x}) \widehat{L}^{\alpha_j^l} (a_{\theta i}^j \widehat{x} + b_{\theta i}^j) d\widehat{x} \right),
\end{aligned}$$

where $a_{\theta i}^j = \frac{h_{K_{\theta i}}^j}{h_{K_\theta}^j}$ and $b_{\theta i}^j = \frac{2}{h_{K_\theta}^j} (x_{K_{\theta i}}^j - x_{K_\theta}^j)$.

Next, we will give numerical proof for different cases. Let us start with the one-dimensional case, i.e., $d = 1$. Where θ, α are all just single indices. The element K_θ can be briefly written as K_j . Besides, We have $\alpha^i = i - 1$ for $i \geq 1$. For $k = 2$, we have $m = 0$ according to the first condition. When taking the center stencil $S_c^1(K_j) = \{K_{j-1}, K_j, K_{j+1}\}$, we have

$$\begin{aligned}
M_{K_j}^2 &= \begin{pmatrix} I_{K_{j-1}}^0 L_{K_j}^0(x) & I_{K_{j-1}}^0 L_{K_j}^1(x) & I_{K_{j-1}}^0 L_{K_j}^2(x) \\ I_{K_j}^0 L_{K_j}^0(x) & I_{K_j}^0 L_{K_j}^1(x) & I_{K_j}^0 L_{K_j}^2(x) \\ I_{K_{j+1}}^0 L_{K_j}^0(x) & I_{K_{j+1}}^0 L_{K_j}^1(x) & I_{K_{j+1}}^0 L_{K_j}^2(x) \end{pmatrix} \\
&= \begin{pmatrix} 1 & b_{j-1} & \frac{3b_{j-1}^2 + a_{j-1}^2 - 1}{2} \\ 1 & 0 & 0 \\ 1 & b_{j+1} & \frac{3b_{j+1}^2 + a_{j+1}^2 - 1}{2} \end{pmatrix}.
\end{aligned}$$

Naturally, the determinant of $M_{K_j}^2$ can be computed as

$$\begin{aligned}
&\det(M_{K_j}^2) \\
&= \frac{3b_{j-1}^2 b_{j+1} - 3b_{j-1} b_{j+1}^2 - b_{j-1} a_{j+1}^2 + b_{j-1} + b_{j+1} a_{j-1}^2 - b_{j+1}}{2}.
\end{aligned}$$

To determine the value of $\det(M_{K_j}^2)$, we need more information. First, the regularity of mesh can induce the following condition

$$0 < a_m < a_{j-q} < a_M, \text{ for } q = 2, 1, -1, -2. \quad (\text{A.3})$$

Moreover, by simple calculation, there are $b_{j-1} = -(1 + a_{j-1})$, $b_{j+1} = 1 + a_{j+1}$. With these informations, the following result can be directly obtained

$$\begin{aligned}\det(M_{K_j}^2)|_{S_c^1} &= 2(a_{j+1} + 1)(a_{j-1} + 1)(a_{j-1} + a_{j+1} + 1) \\ &> 2(a_m + 1)^2(2a_m + 1).\end{aligned}$$

For the backward stencil $S_b^1(K_j) = \{K_{j-2}, K_{j-1}, K_j\}$, the similar determinant property results from the conditions $b_{j-2} = -(1 + 2a_{j-1} + a_{j-2})$, $b_{j-1} = -(1 + a_{j-1})$ and A.3, which is presented as follows,

$$\begin{aligned}\det(M_{K_j}^2)|_{S_b^1} &= 2(a_{j-1} + 1)(a_{j-1} + a_{j-2})(a_{j-1} + a_{j-2} + 1) \\ &> 4a_m(a_m + 1)(2a_m + 1).\end{aligned}$$

In the same way, with the conditions $b_{j+1} = 1 + a_{j+1}$, $b_{j+2} = 1 + 2a_{j+1} + a_{j+2}$ and A.3, we can obtain the determinant property for the forward stencil $S_f^1(K_j) = \{K_j, K_{j+1}, K_{j+2}\}$ as follows,

$$\begin{aligned}\det(M_{K_j}^2)|_{S_f^1} &= 2(a_{j+1} + 1)(a_{j+1} + a_{j+2})(a_{j+1} + a_{j+2} + 1) \\ &> 4a_m(a_m + 1)(2a_m + 1).\end{aligned}$$

The determinant property for the case of $k = 5$ can be deduced following the proof process for $k = 2$. The results are presented in Table A.1.

stencil	$\det(M_{K_j}^5)$
$S_c^1(K_j)$	$252a_{j-1}a_{j+1}(a_{j+1} + 1)^4(a_{j-1} + 1)^4(a_{j-1} + a_{j+1} + 1)^3$ $> 252a_m^2(a_m + 1)^8(2a_m + 1)^4$
$S_b^1(K_j)$	$252a_{j-2}a_{j-1}(a_{j-1} + 1)^4(a_{j-2} + a_{j-1})^4(a_{j-2} + a_{j-1} + 1)^3$ $> 4032a_m^6(a_m + 1)^4(2a_m + 1)^4$
$S_f^1(K_j)$	$252a_{j+1}a_{j+2}(a_{j+1} + 1)^4(a_{j+1} + a_{j+2})^4(a_{j+1} + a_{j+2} + 1)^3$ $> 4032a_m^6(a_m + 1)^4(2a_m + 1)^4$

Table A.1: The determinant of $M_{K_j}^5$.

Next, turn our attention to the two-dimensional case, i.e., $d = 2$. Here, θ, α are all double index with the form (i, j) . The element K_θ can be briefly defined as $K_{i,j} = I_i^1 \times I_j^2$. For $k = 2$, we have $m = 0$. We recall the definition of the two-dimensional stencil, $S^2(K_{i,j}) = S^1(I_i^1) \times S^1(I_j^2)$. Consequently, three different options for one-dimensional stencil produce nine different stencil strategies for two dimension, which are shown as follows,

$$\begin{aligned}S_{cc}^2(K_{i,j}) &= S_c^1(I_i^1) \times S_c^1(I_j^2), \quad S_{cb}^2(K_{i,j}) = S_c^1(I_i^1) \times S_b^1(I_j^2), \quad S_{cf}^2(K_{i,j}) = S_c^1(I_i^1) \times S_f^1(I_j^2), \\ S_{bb}^2(K_{i,j}) &= S_b^1(I_i^1) \times S_b^1(I_j^2), \quad S_{bc}^2(K_{i,j}) = S_b^1(I_i^1) \times S_c^1(I_j^2), \quad S_{bf}^2(K_{i,j}) = S_b^1(I_i^1) \times S_f^1(I_j^2), \\ S_{ff}^2(K_{i,j}) &= S_f^1(I_i^1) \times S_f^1(I_j^2), \quad S_{fc}^2(K_{i,j}) = S_f^1(I_i^1) \times S_c^1(I_j^2), \quad S_{fb}^2(K_{i,j}) = S_f^1(I_i^1) \times S_b^1(I_j^2).\end{aligned}\tag{A.4}$$

Take the stencil $S_{cc}^2(K_{i,j})$ as an example, let us illustrate the proof process. We know that the basis functions of $Q^k(S^2(K_{i,j}))$ are the tensor product of the basis functions of $Q^k(S^1(I_i))$ and $Q^k(S^1(I_j))$. Considering the same product form of the stencils, the coefficient matrix can be expressed by the Kronecker product form

$$M_{K_{i,j}}^2 = M_{I_i}^2 \otimes M_{I_j}^2.$$

Given square matrices A and B with degrees m and n , there is a well-known determinant conclusion for the Kronecker product [15, 31],

$$\det(A \otimes B) = \det(A)^n \det(B)^m.$$

Therefore, we have

$$\det(M_{K_{i,j}}^2) = \det(M_{I_i}^2)^3 \det(M_{I_j}^2)^3.$$

Based on the determinant property in one dimension, we can conclude that the same property also holds for every stencil strategies for two dimension. The same result can be obtained for $k = 5$ according to the fact that

$$\det(M_{K_{i,j}}^5) = \det(M_{I_i}^5)^6 \det(M_{I_j}^5)^6.$$

B Proof of Theorem 1

Proof. The local reconstruction operator R_K^k can be regarded as one interpolation operator. Thus, proving the k -exactness property (3.10) is equivalent to proving the uniqueness of polynomial interpolation problem which has been given by Assumption 1.

With the k -exactness property (3.10), the operator R_K^k can be regarded as a projection operator which projects the Sobolev space $H^{k+1}(S(K))$ on the polynomial space $Q^k(S(K))$. Considering the l_∞ norm $\|\cdot\|_{l_\infty(S(K))}$, as defined in Section 3.2, we have the following property

$$\|R_K^k u\|_{l_\infty(S(K))} = \|u\|_{l_\infty(S(K))}. \quad (\text{B.5})$$

Following [4, Chapter 4.6], there exists an averaged Taylor polynomial $T^{k+1}u \in Q^k(S(K))$ such that

$$\|u - T^{k+1}u\|_{0,\infty,S(K)} \leq Ch^{k+1-\frac{d}{2}}.$$

With (3.8), (B.5), and (3.9), we have

$$\begin{aligned} \|T^{k+1}u - R_K^k u\|_{0,\infty,K} &\leq C\|T^{k+1}u - R_K^k u\|_{0,\infty,S(K)} = C\|R_K^k(T^{k+1}u - u)\|_{0,\infty,S(K)} \\ &\leq C\|R_K^k(T^{k+1}u - u)\|_{l_\infty(S(K))} = C\|T^{k+1}u - u\|_{l_\infty(S(K))} \\ &\leq C\|T^{k+1}u - u\|_{0,\infty,S(K)} \leq Ch^{k+1-\frac{d}{2}}. \end{aligned}$$

Therefore,

$$\|u - R_K^k u\|_{0,\infty,K} \leq \|u - T^{k+1}u\|_{0,\infty,S(K)} + \|T^{k+1}u - R_K^k u\|_{0,\infty,S(K)} \leq Ch^{k+1-\frac{d}{2}},$$

which gives (3.11).

Following (3.11), the L^2 error estimate (3.12) can be derived directly as follows,

$$\|u_h - R_K^k u\|_{0,K} \leq Ch^{\frac{d}{2}} \|u_h - R_K^k u\|_{0,\infty,K} \leq Ch^{k+1}.$$

By the approximation property (2.3), we can choose an approximation polynomial $u_h \in Q^k(S(K))$ such that

$$\|u - u_h\|_{0,K} + h|u - u_h|_{1,K} \leq Ch^{k+1}.$$

With (2.3), (3.12), and the inverse property (2.4), we can derive (3.13) smoothly

$$\begin{aligned} |u - R_K^k u|_{1,K} &\leq |u - u_h|_{1,K} + |u_h - R_K^k u|_{1,K} \\ &\leq Ch^k + Ch^{-1} \|u_h - R_K^k u\|_{0,K} \\ &\leq Ch^k + Ch^{-1} \|u - u_h\|_{0,K} + Ch^{-1} \|u - R_K^k u\|_{0,K} \\ &\leq Ch^k. \end{aligned}$$

Here, the proof is completed. \square

C Proof of Theorem 3

Proof. Given that the exact solution u and \mathbf{q} also satisfies the global weak formulation (4.18), we obtain the following error equation by a simple subtraction

$$\begin{aligned} &((u - u_h)_t, v_h) + \sum_{i=1}^d (q^i - q_h^i, p_h^i) \\ &= \mathcal{H}(u, v_h) - \mathcal{H}(u_h, v_h) + \mathcal{L}(\mathbf{q} - \mathbf{q}_h, v_h) + \sum_{i=1}^d \mathcal{K}^i(u - u_h, p_h^i) + \mathcal{R}(u, v_h) - \mathcal{R}(u_h, v_h). \end{aligned}$$

Here, we denote

$$\begin{aligned} \mathcal{K}(u - u_h, \mathbf{p}_h) &= \sum_{i=1}^d \mathcal{K}^i(u - u_h, p_h^i) \\ &= -\sqrt{\varepsilon} \sum_{i=1}^d ((u - u_h, (p_h^i)_{x_i})_K - \langle u - \hat{u}_h, p_h^i n_i \rangle_{\partial K}) \\ &= -\sqrt{\varepsilon} ((u - u_h, \nabla \cdot \mathbf{p}_h)_K - \langle u - \hat{u}_h, \mathbf{p}_h \cdot \mathbf{n} \rangle_{\partial K}). \end{aligned}$$

Thus a more neat error equation can be described as follows,

$$\begin{aligned} ((u - u_h)_t, v_h) + (\mathbf{q} - \mathbf{q}_h, \mathbf{p}_h) &= \mathcal{H}(u, v_h) - \mathcal{H}(u_h, v_h) + \mathcal{L}(\mathbf{q} - \mathbf{q}_h, v_h) + \mathcal{K}(u - u_h, \mathbf{p}_h) \\ &\quad + \mathcal{R}(u - u_h, v_h). \end{aligned} \tag{C.6}$$

Denote

$$\xi = R^k u - u_h, \quad \xi^e = R^k u - u, \quad \eta = R^k \mathbf{q} - \mathbf{q}_h, \quad \eta^e = R^k \mathbf{q} - \mathbf{q}, \tag{C.7}$$

and take the test function as

$$v_h = \xi, \mathbf{p}_h = \boldsymbol{\eta}. \quad (\text{C.8})$$

We obtain the energy equality

$$((\xi - \xi^e)_t, \xi) + (\boldsymbol{\eta} - \boldsymbol{\eta}^e, \boldsymbol{\eta}) = \mathcal{H}(u, \xi) - \mathcal{H}(u_h, \xi) + \mathcal{L}(\mathbf{q} - \mathbf{q}_h, \xi) + \mathcal{K}(u - u_h, \boldsymbol{\eta}) + \mathcal{R}(u - u_h, \xi). \quad (\text{C.9})$$

Next we will estimate each term on the right-hand side of the energy equality.

To estimate the nonlinear convection term $\mathcal{H}(u, \xi) - \mathcal{H}(u_h, \xi)$, we need to make a *a priori* assumption, for small enough h , we have

$$\|u - u_h\|_0 \leq Ch^{\frac{d+1}{2}}. \quad (\text{C.10})$$

With this assumption, we have $\|u - u_h\|_{0,\infty} \leq Ch^{\frac{1}{2}}$. Moreover, the property (4.21) implies that $\|R^k u - u_h\|_{0,\infty} \leq Ch^{\frac{1}{2}}$.

Here, we have

$$\begin{aligned} & \mathcal{H}(u, \xi) - \mathcal{H}(u_h, \xi) \\ &= \sum_{K \in \mathcal{T}_h} \left((\mathbf{b}(f(u) - f(u_h)), \nabla \xi)_K - \langle \mathbf{b}(f(u) - \hat{f}(u_h)) \cdot \mathbf{n}, \xi \rangle_{\partial K} \right) \\ &= (\mathbf{b}(f(u) - f(u_h)), \nabla \cdot \xi) - \langle \mathbf{b}(f(u) - \hat{f}(u_h)), [\xi] \rangle \\ &= (\mathbf{b}(f(u) - f(u_h)), \nabla \cdot \xi) - \langle \mathbf{b}(f(u) - f(\bar{u}_h)), [\xi] \rangle + \langle \mathbf{b}(f(\bar{u}_h) - \hat{f}(u_h)), [\xi] \rangle \\ &= I + II. \end{aligned}$$

According to [29, Lemma 3.4], the second part can be estimated as

$$II = \langle \mathbf{b}(f(\bar{u}_h) - \hat{f}(u_h)), [\xi] \rangle \leq -\frac{3}{4} \|\mathbf{b}\|_{1,\infty} \langle \alpha(\hat{f}; u_h), [\xi]^2 \rangle + Ch^{2k+1}.$$

Where $\alpha(\hat{f}; u_h)$ is non-negative and bounded, which is defined in [32]. Next, we estimate the first part I . Follow [29, Appendix A.1], I can be divided into six parts as follows,

$$\begin{aligned} I_1 &= (\mathbf{b}f'(u)\xi, \nabla \cdot \xi) + \langle \mathbf{b}f'(u)\bar{\xi}, [\xi] \rangle, \\ I_2 &= \frac{1}{2} \left((\mathbf{b}f''(u)\xi^2, \nabla \cdot \xi) + \langle \mathbf{b}f''(u)\bar{\xi}^2, [\xi] \rangle \right), \\ I_3 &= - \left((\mathbf{b}f'(u)\xi^e, \nabla \cdot \xi) + \langle \mathbf{b}f'(u)\bar{\xi}^e, [\xi] \rangle \right), \\ I_4 &= (\mathbf{b}f''(u)\xi^e\xi, \nabla \cdot \xi) + \langle \mathbf{b}f''(u)\bar{\xi}^e\bar{\xi}, [\xi] \rangle, \\ I_5 &= -\frac{1}{2} \left((\mathbf{b}f''(u)(\xi^e)^2, \nabla \cdot \xi) + \langle \mathbf{b}f''(u)(\bar{\xi}^e)^2, [\xi] \rangle \right), \\ I_6 &= \frac{1}{6} \left((\mathbf{b}f'''_u(\xi - \xi^e)^3, \nabla \cdot \xi) + \langle \mathbf{b}\tilde{f}'''_u(\bar{\xi} - \bar{\xi}^e)^3, [\xi] \rangle \right), \end{aligned}$$

where f'''_u and \tilde{f}'''_u are the factors in the remainder of Taylor expansion of $f(u_h)$ and $f(\bar{u}_h)$ separately. By integration by parts, we can estimate each term now:

- I_1 term

$$I_1 = \frac{1}{2} (\nabla \cdot (\mathbf{b}f'(u)), \xi^2) \leq C \|\xi\|_0^2.$$

- I_2 term

$$I_2 = \frac{1}{6}(\nabla \cdot (\mathbf{b}f''(u))\xi, \xi^2) + \frac{1}{24}\langle \mathbf{b}f''(u)[\xi], [\xi]^2 \rangle.$$

By a Taylor expansion, we have

$$\begin{aligned} f''(u)[\xi] &= f''(u_h)[\xi] + f''_u(u - u_h)[\xi] \\ &= -f''(u_h)[u_h] + f''(u_h)[\xi^e] + f''_u(u - u_h)[\xi] \\ &\leq 8\alpha(\hat{f}; u_h) + 8|[u - u_h]|^2 + f''(u_h)[\xi^e] + f''_u(u - u_h)[\xi]. \end{aligned}$$

Thus,

$$\begin{aligned} I_2 &\leq \frac{1}{3}\|\mathbf{b}\|_{1,\infty}\langle \alpha(\hat{f}; u_h), [\xi]^2 \rangle \\ &\quad + C(\|\xi\|_{0,\infty} + h^{-1}(\|u - u_h\|_{0,\infty}^2 + \|\xi^e\|_{0,\varepsilon_h}^2 + \|\xi\|_{0,\varepsilon_h}^2))\|\xi\|_0 \\ &\leq \frac{1}{3}\|\mathbf{b}\|_{1,\infty}\langle \alpha(\hat{f}; u_h), [\xi]^2 \rangle + C\|\xi\|_0. \end{aligned}$$

- I_3 term

$$\begin{aligned} I_3 &= -(\mathbf{b}f'(u)\xi^e, \nabla \cdot \xi) - \langle \mathbf{b}(f'(u) - f'(\bar{u}_h))\xi^e, [\xi] \rangle - \langle \mathbf{b}f'(\bar{u}_h)\bar{\xi}^e, [\xi] \rangle \\ &\leq C\|\xi\|_0 + 2\langle \mathbf{b}(\alpha(\hat{f}; u_h) + C|[u - u_h]|)\bar{\xi}^e, [\xi] \rangle + Ch^{2k} \\ &\leq \frac{1}{6}\|\mathbf{b}\|_{1,\infty}\langle \alpha(\hat{f}; u_h), [\xi]^2 \rangle + C\|\xi\|_0 + Ch^{2k}. \end{aligned}$$

- $I_4, I_5,$ and I_6 terms

$$\begin{aligned} I_4 &\leq Ch^{-1}\|\xi^e\|_{0,\infty}\|\xi\|_0 \leq C\|\xi\|_0, \\ I_5 &\leq C\|\xi^e\|_{0,\infty}(h^{-1}\|\xi^e\|_0 + h^{-\frac{1}{2}}\|\xi^e\|_{0,\varepsilon_h})\|\xi\|_0 \leq C\|\xi\|_0 + Ch^{2k+2}, \\ I_6 &\leq C\|u - u_h\|_{0,\infty}(h^{-1}(\|\xi\|_0 + \|\xi^e\|_0) + h^{-\frac{1}{2}}\|\xi^e\|_{0,\varepsilon_h})\|\xi\|_0 \\ &\leq C\|\xi\|_0 + Ch^{2k+1}. \end{aligned}$$

Combing with all the above estimates, we can derive that

$$I \leq \frac{1}{2}\|\mathbf{b}\|_{1,\infty}\langle \alpha(\hat{f}; u_h), [\xi]^2 \rangle + C\|\xi\|_0 + Ch^{2k}.$$

Naturally, we have the following estimate

$$\mathcal{H}(u, \xi) - \mathcal{H}(u_h, \xi) \leq -\frac{1}{4}\|\mathbf{b}\|_{1,\infty}\langle \alpha(\hat{f}; u_h), [\xi]^2 \rangle + C\|\xi\|_0 + Ch^{2k}.$$

Then we focus on the diffusion part. We have

$$\begin{aligned} &\mathcal{L}(\mathbf{q} - \mathbf{q}_h, \xi) + \mathcal{K}(u - u_h, \boldsymbol{\eta}) \\ &= -\sqrt{\varepsilon}((\mathbf{q} - \mathbf{q}_h, \nabla \xi) + (u - u_h, \nabla \cdot \boldsymbol{\eta}) - \langle \mathbf{q} - \hat{\mathbf{q}}_h \cdot \mathbf{n}^+, [\xi] \rangle + \langle u - \hat{u}_h, [\boldsymbol{\eta}] \cdot \mathbf{n}^+ \rangle) \\ &= -\sqrt{\varepsilon}((\boldsymbol{\eta} - \boldsymbol{\eta}^e, \nabla \xi) + (\xi - \xi^e, \nabla \cdot \boldsymbol{\eta}) - \langle \hat{\boldsymbol{\eta}} - \hat{\boldsymbol{\eta}}^e \cdot \mathbf{n}^+, [\xi] \rangle + \langle \hat{\xi} - \hat{\xi}^e, [\boldsymbol{\eta}] \cdot \mathbf{n}^+ \rangle) \\ &= \sqrt{\varepsilon}((\boldsymbol{\eta}^e, \nabla \xi) + (\xi^e, \nabla \cdot \boldsymbol{\eta}) - \langle \hat{\boldsymbol{\eta}}^e \cdot \mathbf{n}^+, [\xi] \rangle + \langle \hat{\xi}^e, [\boldsymbol{\eta}] \cdot \mathbf{n}^+ \rangle) \\ &\leq \frac{1}{2}\|\boldsymbol{\eta}\|_0 + C\|\xi\|_0 + Ch^{2k}. \end{aligned}$$

Finally, we estimate the reaction part as follows,

$$\mathcal{R}(u, \xi) - \mathcal{R}(u_h, \xi) = -(r(u) - r(u_h), \xi) = -(r'_u(\xi - \xi^e), \xi) \leq C\|\xi\|_0 + Ch^{2k+2}.$$

With the above estimates and Young's inequality, the energy equation becomes

$$\begin{aligned} \frac{1}{2} \left(\frac{d\|\xi\|_0^2}{dt} + \|\boldsymbol{\eta}\|_0^2 \right) + \frac{1}{4} \|\mathbf{b}\|_{1,\infty} \langle \alpha(\hat{f}; u_h), [\xi]^2 \rangle &\leq (\xi_t^e, \xi) + (\boldsymbol{\eta}^e, \boldsymbol{\eta}) + C\|\xi\|_0 + Ch^{2k} \\ &\leq C\|\xi\|_0 + \frac{1}{4} \|\boldsymbol{\eta}\|_0 + Ch^{2k}. \end{aligned}$$

Thus,

$$\frac{1}{2} \frac{d\|\xi\|_0^2}{dt} + \frac{1}{4} \|\boldsymbol{\eta}\|_0^2 + \frac{1}{4} \|\mathbf{b}\|_{1,\infty} \langle \alpha(\hat{f}; u_h), [\xi]^2 \rangle \leq C\|\xi\|_0 + Ch^{2k}.$$

By the Gronwall inequality and triangle inequality, the proof is completed as follows,

$$\|u - u_h\|_0^2 + \int_0^T \|\mathbf{q} - \mathbf{q}_h\|_0^2(t) dt \leq Ch^{2k}.$$

□

References

- [1] M. Abramowitz and I. A. Stegun. *Handbook of mathematical functions with formulas, graphs, and mathematical tables*. US Government printing office, 1964.
- [2] B. Ayuso and L. D. Marini. Discontinuous Galerkin methods for advection-diffusion-reaction problems. *SIAM Journal on Numerical Analysis*, 47(2):1391–1420, 2009.
- [3] O. Baysal. *Stabilized finite element methods for time dependent convection-diffusion equations*. Izmir Institute of Technology (Turkey), 2012.
- [4] S. C. Brenner, L. R. Scott, and L. R. Scott. *The mathematical theory of finite element methods*. Springer, 2008.
- [5] A. N. Brooks and T. J. Hughes. Streamline upwind/Petrov-Galerkin formulations for convection dominated flows with particular emphasis on the incompressible Navier-Stokes equations. *Computer methods in applied mechanics and engineering*, 32(1-3):199–259, 1982.
- [6] M. Calvo, J. De Frutos, and J. Novo. Linearly implicit Runge–Kutta methods for advection–reaction–diffusion equations. *Applied Numerical Mathematics*, 37(4):535–549, 2001.
- [7] P. G. Ciarlet. *The finite element method for elliptic problems*. SIAM, 2002.
- [8] B. Cockburn, B. Dong, J. Guzmán, M. Restelli, and R. Sacco. A hybridizable discontinuous Galerkin method for steady-state convection-diffusion-reaction problems. *SIAM Journal on Scientific Computing*, 31(5):3827–3846, 2009.

- [9] B. Cockburn, G. E. Karniadakis, and C.-W. Shu. The development of discontinuous Galerkin methods. In *Discontinuous Galerkin Methods*, pages 3–50. Springer, 2000.
- [10] B. Cockburn and C.-W. Shu. TVB Runge-Kutta local projection discontinuous Galerkin finite element method for conservation laws. II. General framework. *Mathematics of computation*, 52(186):411–435, 1989.
- [11] B. Cockburn and C.-W. Shu. The local discontinuous Galerkin method for time-dependent convection-diffusion systems. *SIAM journal on numerical analysis*, 35(6):2440–2463, 1998.
- [12] B. Cockburn and C.-W. Shu. Runge-Kutta discontinuous Galerkin methods for convection-dominated problems. *Journal of scientific computing*, 16(3):173–261, 2001.
- [13] L. B. da Veiga, K. Lipnikov, and G. Manzini. *The mimetic finite difference method for elliptic problems*. Springer, 2014.
- [14] M. Ding, X. Cai, W. Guo, and J.-M. Qiu. A semi-Lagrangian discontinuous Galerkin (DG)–local DG method for solving convection-diffusion equations. *Journal of Computational Physics*, 409:109295, 2020.
- [15] H. V. Henderson, F. Pukelsheim, and S. R. Searle. On the history of the Kronecker product. *Linear and Multilinear Algebra*, 14(2):113–120, 1983.
- [16] P. Houston, C. Schwab, and E. Süli. Discontinuous hp-finite element methods for advection-diffusion-reaction problems. *SIAM Journal on Numerical Analysis*, 39(6):2133–2163, 2002.
- [17] T. J. Hughes, G. Engel, L. Mazzei, and M. G. Larson. A comparison of discontinuous and continuous Galerkin methods based on error estimates, conservation, robustness and efficiency. In *Discontinuous Galerkin Methods*, pages 135–146. Springer, 2000.
- [18] R. J. LeVeque. *Finite difference methods for ordinary and partial differential equations: steady-state and time-dependent problems*. SIAM, 2007.
- [19] J. Li, S. Zhai, Z. Weng, and X. Feng. H-adaptive RBF-FD method for the high-dimensional convection-diffusion equation. *International Communications in Heat and Mass Transfer*, 89:139–146, 2017.
- [20] R. Li and F. Yang. A least squares method for linear elasticity using a patch reconstructed space. *Computer Methods in Applied Mechanics and Engineering*, 363:112902, 2020.
- [21] N. C. Nguyen, J. Peraire, and B. Cockburn. An implicit high-order hybridizable discontinuous Galerkin method for nonlinear convection–diffusion equations. *Journal of Computational Physics*, 228(23):8841–8855, 2009.

- [22] J. Rashidinia, M. Khasi, and G. E. Fasshauer. A stable Gaussian radial basis function method for solving nonlinear unsteady convection-diffusion-reaction equations. *Computers & Mathematics with Applications*, 75(5):1831–1850, 2018.
- [23] H.-G. Roos, M. Stynes, and L. Tobiska. *Robust numerical methods for singularly perturbed differential equations: convection-diffusion-reaction and flow problems*. Springer Science & Business Media, 2008.
- [24] A. Safdari-Vaighani, A. Heryudono, and E. Larsson. A radial basis function partition of unity collocation method for convection-diffusion equations arising in financial applications. *Journal of Scientific Computing*, 64(2):341–367, 2015.
- [25] Z. Sun, J. Liu, and P. Wang. A discontinuous Galerkin method by patch reconstruction for convection-diffusion problems. *Adv. Appl. Math. Mech*, 12(3):729–747, 2020.
- [26] H. Wang, C.-W. Shu, and Q. Zhang. Stability and error estimates of local discontinuous Galerkin methods with implicit-explicit time-marching for advection-diffusion problems. *SIAM Journal on Numerical Analysis*, 53(1):206–227, 2015.
- [27] H. Wang, S. Wang, Q. Zhang, and C.-W. Shu. Local discontinuous Galerkin methods with implicit-explicit time-marching for multi-dimensional convection-diffusion problems. *ESAIM: Mathematical Modelling and Numerical Analysis*, 50(4):1083–1105, 2016.
- [28] H. Wang, Q. Zhang, and C.-W. Shu. Third order implicit–explicit Runge–Kutta local discontinuous Galerkin methods with suitable boundary treatment for convection–diffusion problems with Dirichlet boundary conditions. *Journal of Computational and Applied Mathematics*, 342:164–179, 2018.
- [29] Y. Xu and C.-W. Shu. Error estimates of the semi-discrete local discontinuous Galerkin method for nonlinear convection–diffusion and KdV equations. *Computer methods in applied mechanics and engineering*, 196(37-40):3805–3822, 2007.
- [30] P.-T. Yap and R. Paramesran. An efficient method for the computation of Legendre moments. *IEEE Transactions on Pattern Analysis and Machine Intelligence*, 27(12):1996–2002, 2005.
- [31] H. Zhang and F. Ding. On the Kronecker products and their applications. *Journal of Applied Mathematics*, 2013, 2013.
- [32] Q. Zhang and C.-W. Shu. Error estimates to smooth solutions of Runge–Kutta discontinuous Galerkin methods for scalar conservation laws. *SIAM Journal on Numerical Analysis*, 42(2):641–666, 2004.

